Nuclear Physics A456 (1986) 475–488

COUPLED CHANNELS ANALYSIS OF THE $^{16}O+^{28}Si$ REACTION NEAR THE COULOMB BARRIER

V.N. BRAGIN

I.V. Kurchatov Institute of Atomic Energy, Moscow, USSR

G. POLLAROLO

Dipartimento di Fisica Teorica, Universita di Torino and INFN Sezione di Torino, 10125 Torino, Italy

A. WINTHER

The Niels Bohr Institute, University of Copenhagen, DK-2100 Copenhagen Ø, Denmark

Received 13 January 1986
(Revised 27 February 1986)

Abstract: Good agreement with all the available experimental data on $^{16}O+^{28}Si$ scattering and fusion in the energy range of $E = 21$–38 MeV was obtained with a deformed optical potential consistent with calculations based on nuclear structure information.

1. Introduction

The surprising observation of the anomalous large angle scattering (ALAS) in the $^{16}O+^{28}Si$ system [1]) stimulated numerous investigations of this phenomenon and its theoretical interpretations [2]). Although up to the present time our knowledge has been substantially enriched, still there is as yet no unique and widely accepted understanding of the ALAS, and the subject still attracts considerable attention [3-10]).

In this paper we report the results of a comprehensive analysis of low energy $^{16}O+^{28}Si$ scattering data directly based on available nuclear structure information. To describe the interaction between ^{16}O and ^{28}Si nuclei we thus employ a real part of the optical potential, which is clearly motivated by previous folding-like calculations [11]). We also take into account one-nucleon transfer processes with a microscopically calculated long range imaginary component of the optical potential [12-14]). The effects of the collective excitation of the deformed target nucleus are taken into account explicitly through the coupled channels treatment with a deformation length consistent with measured $B(E2)$ values. Because of the small absorption the optical potential inside the Coulomb barrier is also important. We introduce here a phenomenological imaginary potential for which we are only able to suggest some tentative physical explanation.

Some results on this approach have been published already [15-17]). In the present paper we discuss the model in some more detail and demonstrate how it can be

0375-9474/86/$03.50

successfully used to explain all the available experimental data on the $^{16}O+^{28}Si$ collisions in the incident energy range of $E = 21$–38 MeV. Those include many angular distributions of the elastic and inelastic scattering just above the Coulomb barrier [5,18]) and the corresponding 180° excitation functions [18]) as well. Finally we successfully apply the model to the $^{16}O+^{28}Si$ fusion data [19]) above and below the Coulomb barrier.

2. The optical potential

We describe the interaction between ^{16}O and ^{28}Si nuclei with a deformed optical potential. The spherical equivalent of the real part of the potential is assumed to have the standard Woods-Saxon shape

$$V(r) = -V[1+\exp((r-R_V)/a_V)]^{-1}, \tag{1}$$

with $V = 47.36$ MeV, $R_V = r_V(A_p^{1/3}+A_t^{1/3})$, $r_V = 1.1676$ fm and $a_V = 0.6172$ fm. Those parameters were calculated from the folding-like model of ref. [11]). The two of the parameters (V and a_V) have not been changed in the present calculations. A fine tuning of the r_V parameter (in order to get proper energy dependence of $V(r)$ demanded by the data) is discussed below.

The imaginary part of the potential was assumed to have the following form

$$W(r) = W_1(r) + W_2(r). \tag{2}$$

Here $W_1(r)$ is the long range component of the imaginary part, which takes into account the depopulation of the elastic channel due to one-nucleon transfers. It was calculated with the experimental one-particle level schemes of the colliding nuclei, in the framework of the microscopical model published in refs. [12–14]), at many incident energies in the energy range of $E = 29$–42 MeV. For each energy value the calculated $W_1(r)$ was approximated with a potential of the standard Woods-Saxon form at the nuclear surface

$$W_1(r) = -W_1(E)[1+\exp((r-R_{W_1})/a_{W_1})]^{-1}, \tag{3}$$

with $R_{W_1} = r_{W_1}(A_p^{1/3}+A_t^{1/3})$. The values of $r_{W_1} = 1.08$ fm and $a_{W_1} = 0.55$ fm appeared to be good enough for all the incident energies considered here. The parameter $W_1(E)$ was approximated by the following formula

$$W_1(E) = 0.3 + 0.128(E-\bar{E}) + 0.0145(E-\bar{E})^2, \tag{4}$$

with $\bar{E} = 33.16$ MeV. The formulas (3), (4) provide very good fit to the calculated $W_1(r)$ in the energy range of $E = 29$–42 MeV. For higher energies (4) overestimates the absorption, but this is not important for the present calculations. For lower energies $E \leq 29$ MeV we set $W_1(E) = 0$. The component $W_1(r)$ is illustrated in fig. 1.

The second term $W_2(r)$ in (2) stands for the short range component of the imaginary part. It was assumed to have the standard Wood-Saxon form

$$W_2(r) = -W_2(E)[1+\exp((r-R_{W_2})/a_{W_2})]^{-1}, \tag{5}$$

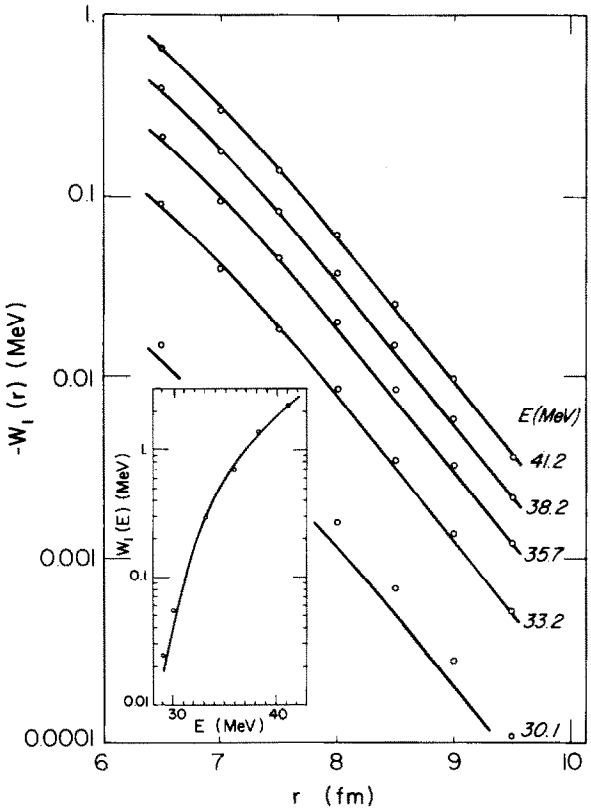

Fig. 1. The long range component of the imaginary part of the optical potential. Shown are the microscopically calculated values (points) at several incident energies and the Woods-Saxon fit to them (solid curves). Inset is shown the energy dependence of the depth $W_1(E)$: individual fit at several energies (points) and smooth fit (solid curve) defined by the formula (4).

with the two parameters: $R_{W_2} = 0.85(A_p^{1/3} + A_t^{1/3})$ fm and $a_{W_2} = 0.2$ fm, which were kept constant in the present calculations. The depth of this potential $W_2(E)$ was treated as a freely adjustable parameter. Its energy dependence and possible physical meaning of $W_2(r)$ are discussed below.

For the Coulomb component of the ion-ion potential we have adopted the standard expression with the parabolic approximation in the inner region identified with the radius $R_c = r_c(A_p^{1/3} + A_t^{1/3})$ fm. In most cases the elastic scattering angular distribution is insensitive to the value of r_c because of the large value of the imaginary potential. This is clearly not the case for the $^{16}O + ^{28}Si$ where the potential is quite transparent. On the other hand it is well known that the Coulomb interaction between two extended charge distributions with radii R_1 and R_2 follows the $1/r$ law to distances well below $R_1 + R_2$. In our case we set $r_c = 1.05$ fm and keep this value fixed throughout all the calculation.

3. The model

Since in the $^{16}O+^{28}Si$ scattering system the target nucleus is well known to be strongly deformed, one should treat its collective excitation explicitly in the framework of the coupled channels formalism. We assume that the target nucleus has a static quadrupole deformation, and that its rotation can be described in the framework of the collective rotational model. To take this into account we deform the optical potential in the following way

$$R_V(\theta, \phi) = r_V A_p^{1/3} + r_V A_t^{1/3}[1 + \beta_2 Y_{20}(\theta, \phi)], \tag{6}$$

where β_2 is the deformation parameter of ^{28}Si (see below). The same formula is also used for the two radii of the imaginary part of the potential. The same deformation parameter β_2 is used for the calculation of the Coulomb excitation of the target.

Bearing in mind the influence of the deformation on the curvature of the target nucleus surface at the point of contact with the projectile we employ the following expression for the depth of the real part of the potential [11])

$$V(\theta, \phi) = V[1 - 2A_p^{1/3}/(A_p^{1/3} + A_t^{1/3})\beta_2 Y_{20}(\theta, \phi)]. \tag{7}$$

This correction reduces the effect of the deformation by about 15%.

In the present calculations we take into account the first two excited states of the target: 2^+ (1.78 MeV) and 4^+ (4.62 MeV), and assume them to be members of the $K = 0$ rotational band built on the ground state of ^{28}Si. Under this assumption we employ the 0^+-2^+-4^+ coupling scheme and exact multipole expansion of the deformed optical potential to calculate the diagonal distorting potentials and the off-diagonal couplings illustrated in fig. 2. The reorientation effects for 2^+ and 4^+ excited states are also included. We discuss the validity of the assumed coupling scheme below. The calculations were performed with an appropriately modified version of the computer code CHUCK [20]).

4. Analysis of the experimental data

4.1. FIT TO THE SCATTERING DATA AT $E = 33.16$ MeV

Two sorts of the experimental data are available at the incident energy of $E = 33.16$ MeV, which corresponds to the position of the first pronounced peak in the experimental 180° elastic scattering excitation function [18]). Those are the elastic and inelastic (2^+, 1.78 MeV) scattering angular distributions [18]), covering the whole angular range.

The two parameters ($W_2(E)$ and β_2) were systematically adjusted to obtain the best possible simultaneous fit to the elastic and inelastic scattering data. This ended with the following values of the adjusted parameters: $W_2(E) = 3.6$ MeV and $\beta_2 =$

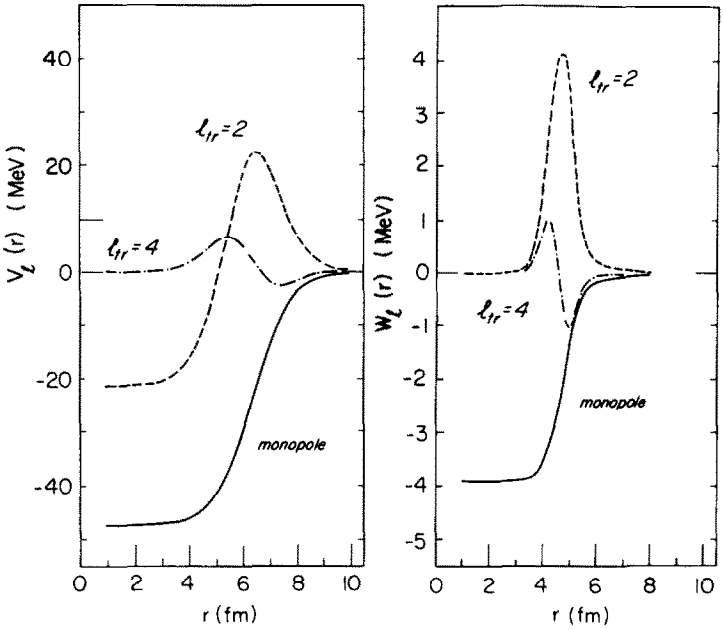

Fig. 2. Exact multipole expansion of the deformed optical potential calculated at $E = 33.16$ MeV. Shown are the monopole, quadrupole and hexadecapole (neglected in the present calculations) components of the real and imaginary parts of the potential.

-0.47. This value of the deformation parameter β_2 was fixed and never changed in the present calculations.

It is worth mentioning that there exists a certain ambiguity in the determination of those two parameters. For example, one can get fit of the same quality to the elastic scattering data with $W_2(E) = 4.0$ MeV and $\beta_2 = -0.41$, which is a more conventional value of β_2 at the time. But the fit to the inelastic scattering data will become worse although still reasonable. There exists also a certain ambiguity between the two parameters $W_1(E)$ and $W_2(E)$. For example, if one sets $W_1(E) = 0.6$ MeV (instead of $W_1 = 0.3$ MeV as expected from formula (4)) one can easily compensate this change by setting $W_2(E) = 3.1$ MeV with the same quality of the fit.

4.2. ELASTIC AND INELASTIC SCATTERING DIFFERENTIAL CROSS SECTIONS

The fit to the data at $E = 33.16$ MeV, which was obtained in the previous subsection, is shown in figs. 3 and 4 by the solid curves in comparison with the experimental data [18]). We also calculated angular distributions of the elastic and inelastic scattering at several incident energies in the energy range of $E = 29$–38 MeV. First, we used the same parameters as described above (for the case of $E = 33.16$ MeV) for all incident energies. The only energy-dependent ingredient of those calculations was

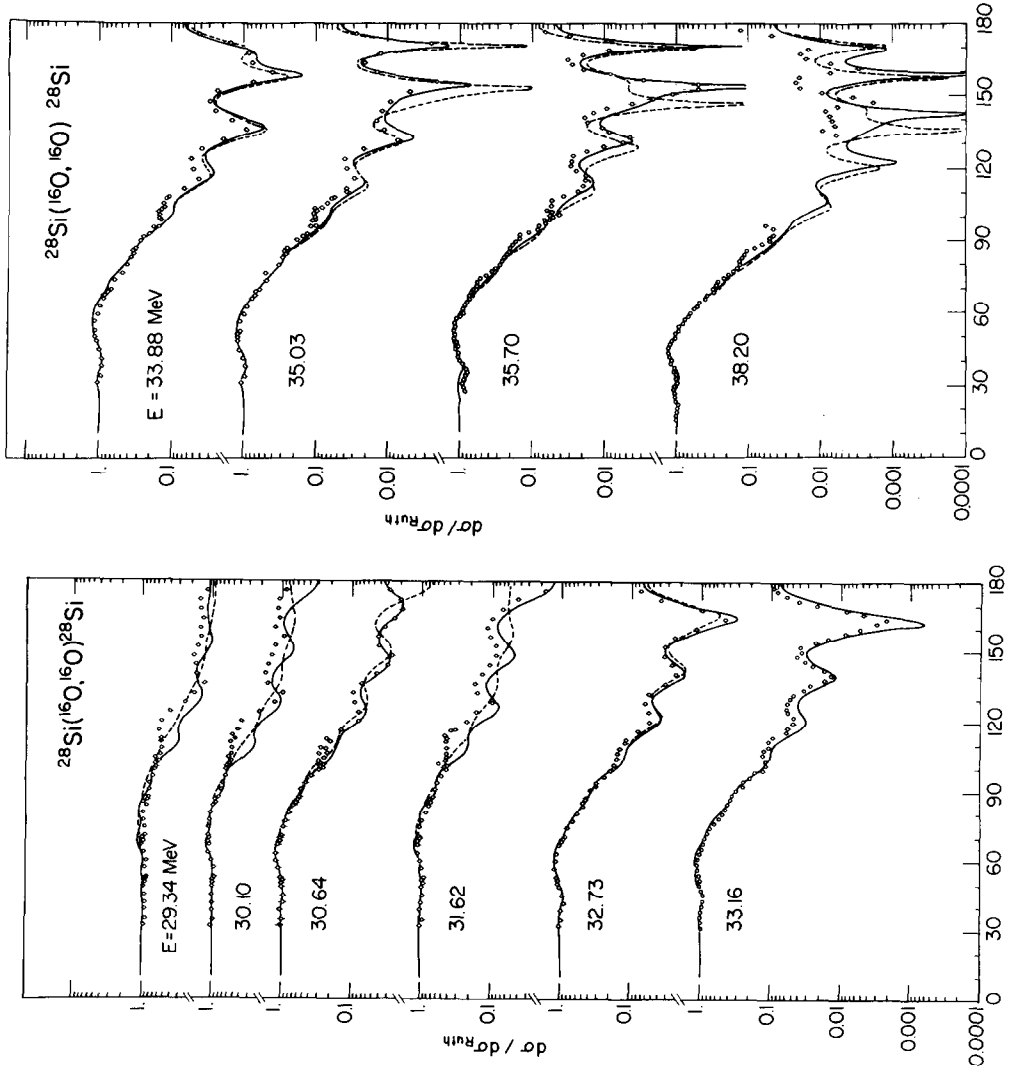

Fig. 3. Elastic scattering angular distributions for $^{16}O + ^{28}Si$ system in the incident energy range of $E = 29$–38 MeV. Shown are the cross sections calculated with energy independent real part of the potential (dashed curves) and those calculated with energy-dependent reduced radius r_V (solid curves). The experimental data are taken from refs.[5,10]).

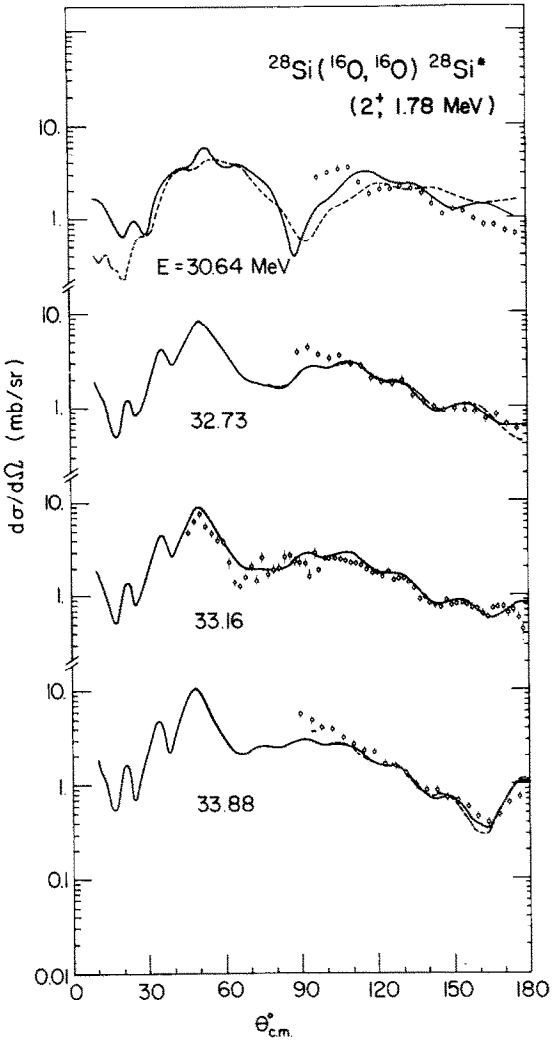

Fig. 4. Inelastic (2^+, 1.78 MeV) scattering angular distributions for $^{16}O+^{28}Si$ system. Notation is the same as in fig. 3.

the depth of the long range component of the imaginary part that follows (cf. eq. (4)) from the calculation of $W_1(E)$. The results are shown by the dashed curves in figs. 3 and 4 in comparison with the data [5,19]). One can observe in fig. 3 a rather systematic shift of the calculated angular distributions to the left comparing to the data at $E \geqslant 33.16$ MeV. Note also large discrepancy of the calculated and experimental elastic scattering cross sections at lower energies.

We made a smooth adjustment of one parameter, namely the reduced radius r_V of the real part of the potential, in order to improve the fit to the data. We found that it was possible to do it in a very systematic way by assuming the following

energy dependence of the radius

$$r_V = \bar{r}_V[1 - 0.00384\,(E - \bar{E}) + 0.000433\,(E - \bar{E})^2]\,, \tag{8}$$

with $\bar{r}_V = 1.1676$ fm and $\bar{E} = 33.16$ MeV.

The results of the calculations with the energy dependent r_V are shown in figs. 3 and 4 by the solid curves. A striking systematic improvement of the fit at all incident energies indicates that the energy dependence of the real part of the potential observed in the present calculations is clearly demanded by the data. This change of the potential does not seem likely to be accounted for by possible experimental uncertainties in the determination of the incident energies. The formula (8) is used for all of the calculations discussed below.

It should be observed that the energy dependence of r_V is very small indeed. Thus in the energy range of $E = 29$–38 MeV the change of the radius never exceeds 2%. There was no need in our calculations to change the depth of the short range component of the imaginary part but for the lowest three incident energies $E = 29.34$, 30.10 and 30.64 MeV, for which we set $W_2(E) = 2.3$, 2.1 and 1.7 MeV respectively in order to enhance a little the oscillations of the calculated cross sections at the largest angles. But this does not affect the positions of the peaks in the calculated angular distributions. We found this change of $W_2(E)$ with energy rather consistent with what we observed later when calculating the 180° excitation functions and the fusion cross section below the Coulomb barrier.

4.3. 180° EXCITATION FUNCTIONS AND FUSION CROSS SECTION

Next we calculated the 180° excitation functions for the elastic and inelastic (2^+, 1.78 MeV) scattering and show the results in fig. 5 in comparison with the experimental data [18]). Bearing in mind the reported experimental procedure we averaged our calculated excitation functions over the last 5° in the vicinity of $\theta = 180°$.

For the incident energies $E \geqslant 29$ MeV in these calculations we used the same parameters as described above. For lower energies we found it necessary to adjust the depth of the short range component of the imaginary part in order to get a better fit to the data on the 180° elastic excitation function below the Coulomb barrier. Finally we found that in the energy range of $E = 21$–28 MeV the depth $W_2(E)$ varies smoothly and becomes $W_2(E) = 0.5$ MeV at $E = 21$ MeV. The energy dependence of $W_2(E)$ is illustrated in fig. 6.

We finally calculated the fusion cross section for the $^{16}O + ^{28}Si$ system in the energy range of $E = 21$–40 MeV. The cross section was defined as follows

$$\sigma_{\text{fus}} = \sigma_{\text{abs}} - \sigma(2^+) - \sigma(4^+)\,, \tag{9}$$

where σ_{abs} is the standard CC absorption cross section, and $\sigma(2^+)$, $\sigma(4^+)$ stand for the total cross sections of the excitation of the target nucleus into its 2^+ and 4^+ states respectively. In (9) we neglected the contribution from transfer channels which

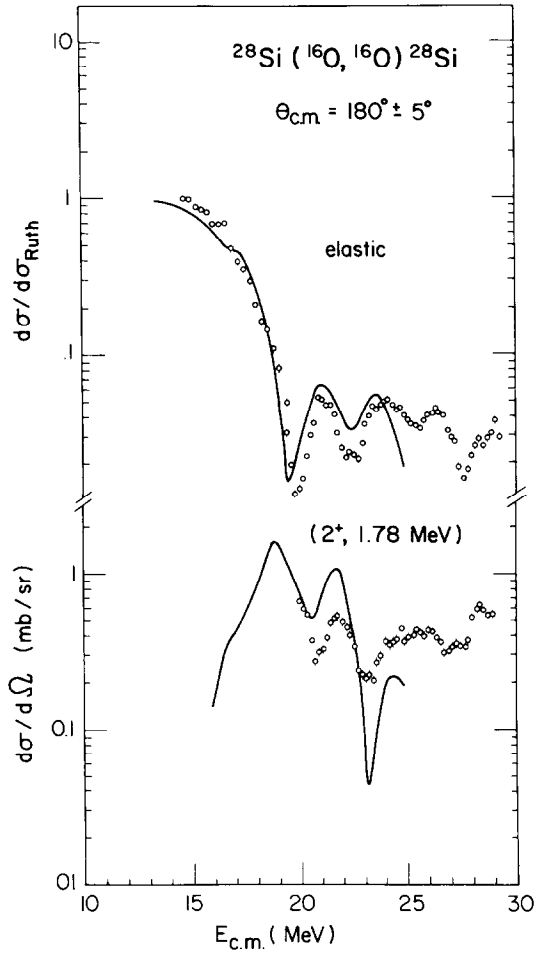

Fig. 5. 180° excitation functions for elastic and inelastic $^{16}O+^{28}Si$ scattering. The experimental data are taken from ref. [18]).

is small compared to σ_{fus} [ref. [23])]. We show the results in fig. 7 in comparison with the experimental data [19]). It should be observed that these results were obtained in a straightforward way from the same calculations as the angular distributions and the excitation functions discussed in the two previous subsections.

5. Discussion

In order to achieve a better understanding of the qualitative features of the present analysis we calculated the angular distribution of the $^{16}O+^{28}Si$ elastic scattering at $E = 33.16$ MeV within the framework of the pure optical model and show the results in fig. 8 by the solid curve. In these calculations the optical potential was defined

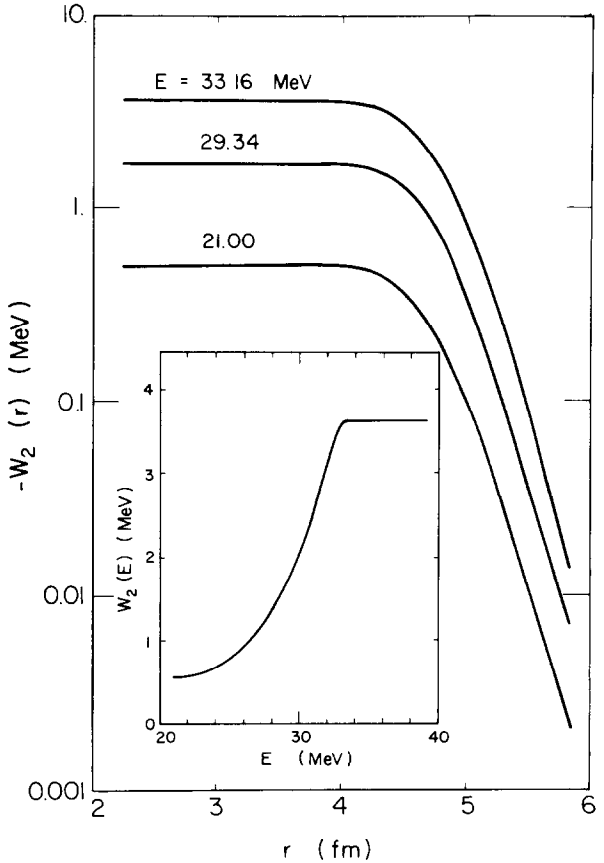

Fig. 6. The short range component of the imaginary part of the optical potential is shown at several incident energies. Inset is shown the energy dependence of its depth $W_2(E)$.

as above (by the formulas (1)-(5)) but the deformation of the target nucleus was neglected. We also made decomposition of the elastic scattering amplitude into its near- and far-side components (performed with an appropriately modified version of the computer code SPI-GENOA [21]))

$$f(\theta) = f_N(\theta) + f_F(\theta)\,, \tag{10}$$

and show in fig. 8 the corresponding cross sections $\sigma_{N,F}(\theta) = |f_{N,F}(\theta)|^2$. Without the coupling effects we obtain a rather smooth angular distribution with suppressed and shifted oscillations in comparison to those calculated within the coupled channels approach. In the whole angular range the cross section is dominated by its near-side component, which corresponds to the positive scattering angles. The far-side component of the cross section is very small and gives rise to slight oscillations in the cross section due to the interference of the two components.

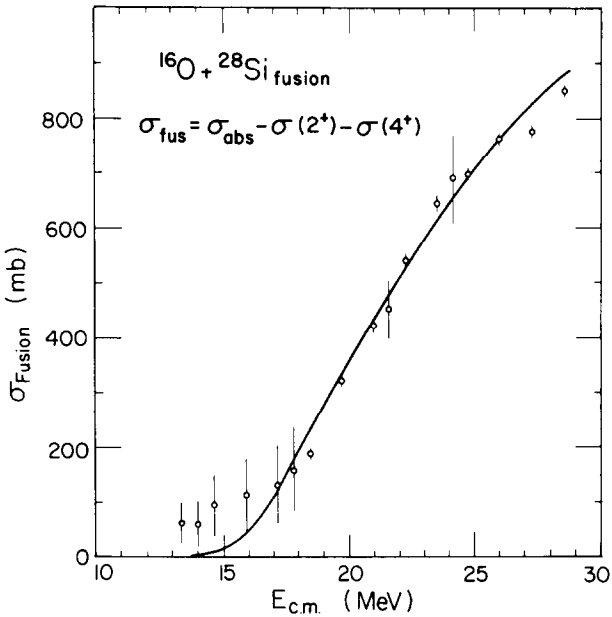

Fig. 7. Fusion cross section for $^{16}O + ^{28}Si$ system. The experimental data are taken from ref. [19]).

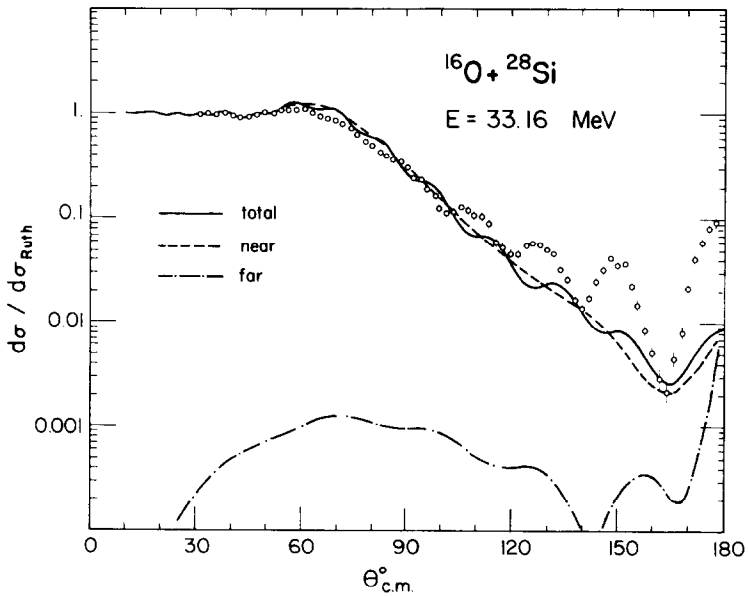

Fig. 8. Angular distribution of elastic $^{16}O + ^{28}Si$ scattering at $E = 33.16$ MeV calculated in the framework of the optical model and its near/far-side decomposition.

Switching on of the couplings creates a more pronounced oscillatory structure of the angular distribution. This can be classically understood by the fact that in the coupled motion the projectile may be caught for a while behind the Coulomb barrier [17]). Surface transparency implies a large probability for the system to return back to the entrance channel. This point is illustrated by fig. 9 in which we show at several incident energies the angular momentum dependence of the magnitude of the elastic scattering matrix, obtained from the CC calculations discussed in subsect. 4.2.

We would like to remind here that the real part of the potential (1) is based on folding-like calculations which are only valid for the surface region. In the presence of surface transparency the results of the calculations are rather sensitive to the details of the potential inside the target nucleus. At such small separations one might expect a short range repulsion [6,9,10]) due to the Pauli principle effects, which prevents the colliding nuclei from interpenetration. In the present calculations a phenomenological correction to the optical potential is represented by a short range component of the imaginary part $W_2(r)$. It can be tentatively understood as arising (partially at least) from α-transfer processes [15-17]). Its rather short range and small diffuseness are clearly indicating this possibility. Together with the long range

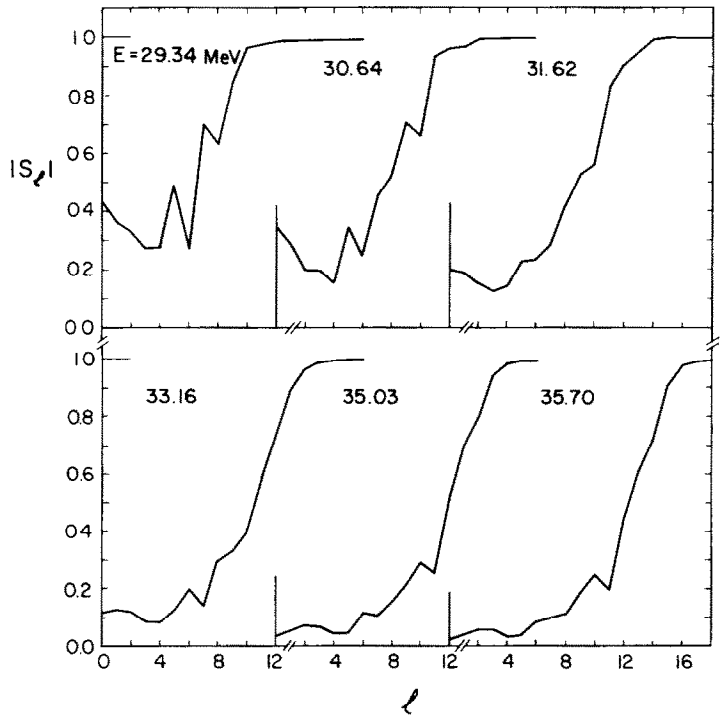

Fig. 9. The magnitude of the scattering matrix as a function of the angular momentum is shown at several incident energies.

absorption it also serves as a sink for fusion reactions. Because of its small diffuseness it also gives rise to some reflection. A systematic investigation of a combined real and imaginary short range potential is in progress.

The observed energy dependence of the real part of the potential is not understood. We made an attempt to calculate the polarization correction $\Delta V_1(r)$ to the real part of the potential due to one-nucleon transfer processes (the model will be published elsewhere [22])) and found that its strength and a very slow energy dependence does not seem to explain the phenomenologically established tendency. It should be noted however that the present calculations are very sensitive to all parameters, and that the energy variation of $\Delta V_1(r)$ may compensate for some other defaults in the model.

We conclude this section with the discussion of the rotational model employed in the present calculations. In fact the inclusion of the 6^+(8.54 MeV) excited state of ^{28}Si in our model also affects the results of the calculations considerably. It was shown in ref. [17]) that this change could be partially compensated by some readjustment of the real part of the potential but with a worse fit to the data. One should however bear in mind that ^{28}Si could hardly be considered to be a good rotor as far as 6^+ and higher excited states are concerned. The procedure used in the present paper of cutting the rotational band at the 4^+ state should be improved and with more experimental information one could hope to use B(E2) values which in a more realistic way change gradually for the transitions between higher states [16]).

6. Conclusion

An excellent fit to all the available experimental data on the $^{16}O+^{28}Si$ scattering and fusion in the incident energy range of $E = 21$–38 MeV was obtained with a deformed optical potential consistent with nuclear structure information. Although many questions still need further investigations we believe it to be well demonstrated that an explicit treatment of the coupling effects is necessary to obtain an authentic explanation of the ALAS phenomenon in the collisions of strongly deformed heavy ions in the vicinity of the Coulomb barrier.

We are very thankful to J. Barrette, J.V. Maher and M.C. Mermaz for the experimental data. V.N. Bragin and G. Pollarolo acknowledge the hospitality of the NBI during their stay in Copenhagen.

References

1) P. Braun-Munzinger, G.M. Berkowitz, T.M. Cormier, C.M. Jachcinski, J.W. Harris, J. Barrette and M.J. LeVine, Phys. Rev. Lett. **38** (1977) 944
2) P. Braun-Munzinger and J. Barrette, Phys. Reports, **87** (1982) 209
3) V. Shkolnik, D. Dehnhard and M.A. Franey, Phys. Rev. **C28** (1983) 717
4) S. Kahana, J. Barrette, B. Berthier, E. Chavez, A. Greiner and M.C. Mermaz, Phys. Rev. **C28** (1983) 1393

5) M.C. Mermaz, E.R. Chavez-Lomeli, J. Barrette, B. Berthier and A. Greiner, Phys. Rev. **C29** (1984) 147
6) V.N. Bragin, Sov. J. Nucl. Phys. **37** (1983) 722
7) A.M. Kobos, G.R. Satchler and R.S. Mackintosh, Nucl. Phys. **A395** (1983) 248
8) A.M. Kobos and G.R. Satchler, Nucl. Phys. **A427** (1984) 589
9) V.N. Bragin and R. Donangelo, Nucl. Phys. **A433** (1985) 495
10) V.N. Bragin and R. Donangelo, Phys. Rev. **C32** (1985) 2176
11) R.A. Broglia and A. Winther, Heavy ion reactions, vol. 1 (Benjamin/Cummings, 1981)
12) R.A. Broglia, G. Pollarolo and A. Winther, Nucl. Phys. **A361** (1981) 307
13) G. Pollarolo, R.A. Broglia and A. Winther, Nucl. Phys. **A406** (1983) 369
14) J.M. Quesada, R.A. Broglia, V.N. Bragin and G. Pollarolo, Nucl. Phys. **A428** (1984) 305c
15) A. Winther, Nucl. Phys. **A409** (1983) 21c
16) S. Kahana, G. Pollarolo, J. Barrette, A. Winther and R.A. Broglia, Phys. Lett. **133B** (1983) 283
17) G. Pollarolo and R.A. Broglia, Nuovo Cim. **81A** (1984) 278
18) P. Braun-Munzinger, G.M. Berkowitz, M. Gai, C.M. Jachcinski, T.R. Renner, C.D. Uhlhorn, J. Barrette and M.J. LeVine, Phys. Rev. **C24** (1981) 1010
19) W.J. Jordan, J.V. Maher and J.C. Peng, Phys. Lett. **87B** (1979) 38
20) P.D. Kunz, CHUCK, a coupled channels code, unpublished
21) F. Perey, SPI-GENOA, an optical model search code, unpublished
22) C.H. Dasso, S. Landowne, G. Pollarolo and A. Winther, to be published
23) J.V. Maher, K.A. Erb and R.W. Miller, Phys. Rev. **C7** (1973) 651